Direct photon pair production at the LHC to $\mathcal{O}(\alpha_s)$ in TeV scale gravity models

M.C. Kumar[a,b 1], **Prakash Mathews**[b 2],
V. Ravindran[c 3], **Anurag Tripathi**[c 4]

a) Saha Institute of Nuclear Physics, 1/AF Bidhan Nagar, Kolkata 700 064, India.

b) School of Physics, University of Hyderabad, Hyderabad 500 046, India.

c) Regional Centre for Accelerator-based Particle Physics,
Harish-Chandra Research Institute, Chhatnag Road, Jhunsi, Allahabad, India.

Abstract

The first results on next-to-leading order QCD corrections to production of direct photon pairs in hadronic collisions in the extra dimension models— ADD and RS are presented. Various kinematical distributions are obtained to order α_s in QCD by taking into account all the parton level subprocesses. Our Monte Carlo based code incorporates all the experimental cuts suitable for physics studies at the LHC. We estimate the impact of the QCD corrections on various observables and find that they are significant. We also show the reduction in factorisation scale uncertainity when $\mathcal{O}(\alpha_s)$ effects are included.

[1]mc.kumar@saha.ac.in
[2]prakash.mathews@saha.ac.in
[3]ravindra@hri.res.in
[4]anurag@hri.res.in

1 Introduction

The hierarchy problem is a long standing problem and has been the main motivation for physics beyond the SM. The hierarchy between the electroweak scale and the Planck scale has in the past been addressed by modifying the particle content of the theory— supersymmetry and technicolor belong to this category. A paradigm shift in this approach was proposed by Arkani-Hamed, Dimopoulos and Dvali (ADD) [1], wherein they modified only the gravity sector. Though the idea of extra dimensions existed since the 1900s, all models assumed that gravity together with other interactions could live in the full extra dimensions. Consistency with the experimental observations, demands that these extra dimensions be very small. The ADD scenario explored the possibility of allowing only gravity to probe all dimensions and studied the constraints on the size of the extra dimensions. It turns out that for more then one extra dimensions, their size could be large without contradicting any known experimental observations and consequently explain the weakness of gravity in 4-dimensions. An alternate solution of the hierarchy problem was suggested by Randall and Sundrum [2] with a single extra dimension in an Anti-de-Sitter (AdS_5) metric. The ADD and RS models used the geometry of the extra dimensions to account for the hierarchy between the electroweak scale and the Planck scale. In order that these models are consistent with present experimental length scale probed at colliders, it is essential that these extra dimensions remain hidden. Various extra dimensional models have used different physical mechanisms to hide them. The extra dimensions could be small and compact wherein all the SM fields are allowed to propagate, or alternatively the brane world scenarios where the SM particles are confined to the brane. In the brane world scenarios the extra dimensions could be of macroscopic size (ADD) without contradiction with present experiments. ADD and RS are both brane-world scenarios.

In the ADD case the compactified extra dimensions are flat and could be large. It follows from Gauss Law that the effective Planck scale M_P in 4-dimension is related

to a fundamental scale M_S in $4+d$-dimension through the volume of the compactified d extra spatial dimensions [1]. The hierarchy between the Planck scale and the electroweak scale (M_W) is solved by assuming $M_S \approx M_W$. A viable mechanism to hide the extra spatial dimensions, is to introduce a 3-brane with negligible tension and localise the SM particles on it. Only gravity is allowed to propagate in all dimensions. The d spatial dimensions are compactified on a torus of common circumference R. The spectrum consists of the SM fields and a tower of Kaluza-Klein (KK) modes of the graviton fields. The number of extra spacial dimension possible is $d \geq 2$ from current experimental limits on deviation from inverse square law [3].

This was the first extra dimension model in which the compactified dimensions could be of macroscopic size and consistent with present experiments. In this model, new physics can appear at a mass scale of the order of a TeV. The interaction of the KK modes $h_{\mu\nu}^{(\vec{n})}$ with the SM fields localised on the 3-brane is given by

$$\mathcal{L} = -\frac{\kappa}{2} \sum_{\vec{n}=0}^{\infty} T^{\mu\nu}(x)\, h_{\mu\nu}^{(\vec{n})}(x)\ , \tag{1}$$

where $\kappa = \sqrt{16\pi}/M_P$ and $T^{\mu\nu}$ is the energy-momentum tensor of the SM fields on the 3-brane. The zero mode corresponds to the usual 4-dimensional massless graviton. The KK modes are M_P suppressed but the high multiplicity could lead to observable effects. In a process involving a virtual exchange of KK modes from SM particles, the sum of KK propagators $\mathcal{D}(Q^2)$ is given by

$$\begin{aligned} \kappa^2 \mathcal{D}(Q^2) &= \kappa^2 \sum_n \frac{1}{Q^2 - m_n^2 + i\epsilon}\ , \\ &= \frac{8\pi}{M_S^4} \left(\frac{Q}{M_S}\right)^{(d-2)} \Big[-i\pi + 2I(\Lambda/Q) \Big]\ , \end{aligned} \tag{2}$$

the integral $I(\Lambda/Q)$ is a result of the summation over the non-resonant KK modes and the term proportional to π is due to the resonant production of a single KK modes [4]. Λ is the explicit cut-off on the KK sum which is identified with the scale of the extra dimension theory M_S [4,5]. The κ^2 suppression in a virtual exchange is compensated for by the high multiplicity, after the KK modes are summed over. The ADD scenario

raises the exciting possibility of observing quantum gravity at the LHC. Basic collider signals of the ADD scenario could be (a) real KK mode production resulting in missing energy in association with a SM gauge boson or a hadronic jet or (b) virtual KK mode exchange which could lead to deviations from the SM predictions. Interesting phenomenological consequence have been considered in [4–7].

In the RS model there is only one extra spacial dimension and the extra dimension is compactified to a circle of circumference $2L$ and further orbifolded by identifying points related by $y \to -y$. Two brane are placed at orbifold fixed points, $y = 0$ with positive tension called the Planck brane and a second brane at $y = L$ with negative tension called the TeV brane. For a special choice of parameters, it turns out that the 5-dimensional Einstein equations have a warped solution for $0 < y < L$ with metric $g_{\mu\nu}(x^\rho, y) = \exp(-2ky)\ \eta_{\mu\nu}$, $g_{\mu y} = 0$ and $g_{yy} = 1$. This space is not factorisable and has a constant negative curvature— AdS_5 space-time. k is the curvature of the AdS_5 space-time and $\eta_{\mu\nu}$ is the usual 4-dimensional flat Minkowski metric. In this model the mass scales vary with y according to the exponential warp factor. If gravity originates on the brane at $y = 0$, TeV scales can be generated on the brane at $y = L$ for $kL \sim 10$. The apparent hierarchy is generated by the exponential warp factor and no additional large hierarchies appear. The size of the extra dimension is of the order of M_P^{-1}. Further it has been showed that [8] the value of kL can be stabilised without fine tuning by minimising the potential for the modulus field which describes the relative motion of the two branes. In the RS model graviton and the modulus field can propagate the full 5-dimensional space time while the SM is confined to the TeV brane. The 4-dimensional spectrum contains the KK modes, the zero mode is M_P suppressed while the excited modes are massive and are only TeV suppressed. The mass gap of the KK modes is determined by the difference of the successive zeros of the Bessel function $J_1(x)$ and the scale $m_0 = k\ e^{-\pi kL}$. As in the ADD case the phenomenology of the RS model concerns the effect of massive KK modes of the graviton, though the spectrum of the KK mode is quite different.

In the RS model the massive KK modes $h^{(n)}_{\mu\nu}(x)$ interacts with the SM fields

$$\mathcal{L}_{int} \sim -\frac{1}{M_P} T^{\mu\nu}\, h^{(0)}_{\mu\nu} - \frac{1}{M_P\, e^{-\pi kL}} \sum_{n=1}^{\infty} T^{\mu\nu}\, h^{(n)}_{\mu\nu}\ , \tag{3}$$

where the energy-momentum tensor $T^{\mu\nu}$ of the SM fields lives on the 3-brane at $y = L$ and its coupling to the massive KK modes could be TeV suppressed if $kL \sim 10$. The masses of $h^{(n)}_{\mu\nu}$ are given by $M_n = x_n\ k\ e^{-\pi kL}$, where x_n are the zeros of the Bessel function $J_1(x)$. In this model there are two parameters which are $c_0 = k/M_P$, the effective coupling and m_1 the mass of the first KK mode. Except for an overall warp factor the Feynman rules of RS are the same as those of the ADD model. In the RS case since the spectrum is massive and its spacing is determined by x_n, the summation of the propagator is given by [9]

$$\begin{aligned} \mathcal{D}(Q^2) &= \sum_n \frac{1}{s - M_n^2 + iM_n\Gamma_n}\ , \\ &= \frac{1}{m_0^2} \sum_n \frac{X^2 - X_n^2 - i\frac{\Gamma_n}{m_0} X_n}{(X^2 - X_n^2)^2 + \frac{\Gamma_n^2}{m_0^2} X_n^2}\ , \end{aligned} \tag{4}$$

where $X = \sqrt{s}/m_0$ and $X_n = M_n/m_0$. The summation over n is kinematically bounded. Further the RS KK mode of mass M_n if decays only to SM particles, the decay width Γ_n is fixed. The signal is now resonant enhancement over the SM predictions and is very distinct compared to the ADD case which leads to an enhancement of the tail for say the invariant mass distribution.

Production of photon pairs at hadronic colliders is an important process as it provides a clean channel not only to test the predictions of the SM but also of any new physics beyond it. An extensive study of this process exists in the literature [11] in the context of light Higgs-boson searches as a light Higgs Boson decays dominantly to two photons. This channel has also been widely used for various beyond SM studies [12]. Recently we completed a next-to-leading order computation for this process in the context of theories with large extra-dimension and unparticle model [16]. The present paper aims at a full next-to-leading order computation for production of isolated direct photon pairs at the LHC at $\sqrt{S} = 14$ TeV, and to obtain various kine-

matical distributions with experimental cuts imposed on the photons. All the details of the calculation are presented here which were not presented in previous publications [16, 17]. The estimate of enhancement over LO result and the improvement in scale uncertainties in going from a LO result to a NLO result are the main motivations for this work. In [13], QCD radiative corrections beyond LO to Drell-Yan process in gravity mediated models were first studied and it was found to be large. Subsequently, they were used (see [14, 15]) to constrain the model parameters.

The NLO calculation presented here uses both analytical and Monte Carlo integration methods. It is easy to impose experimental cuts in a Monte Carlo calculation than a fully analytical computation. Our code is based on the method of *two cut-off phase space slicing* [19] to deal with various singularities appearing in the NLO computation and to implement the numerical integrations over phase space. It has been applied to diphoton production in [20]. This method is nicely reviewed in [21]. All the analytical results presented in this paper were evaluated using the algebraic manipulation program FORM [18].

At the lowest order in α_s ie., at α_s^0, two photons in the final state are produced in quark anti-quark annihilation subprocess $q\overline{q} \to \gamma\gamma$ in the SM. For low invariant mass photon pairs $gg \to \gamma\gamma$, although of order α_s^2, is comparable to $q\overline{q} \to \gamma\gamma$. This is due to the large gluon densities at small x. In light Higgs boson search studies this subprocess plays an important role, and it is treated formally as a leading order contribution although it is of order α_s^2 [11, 22] and is really a next-to-next-to leading order contribution. However, it falls rapidly with increasing invariant mass and in the mass range of interest for the TeV scale gravity models, it need not be included at LO. We have demonstrated in [17] that this subprocess in the SM is few orders of magnitude smaller than that of $q\bar{q}$ when $Q > 500$ GeV. This subprocess amplitude can interfere with the gluon initiated LO subprocess in ADD (also in RS) giving order α_s contribution which is included in our study. In addition order κ^2 gravity mediated Feynman diagrams fig.(1) $qq \to \gamma\gamma$ and $gg \to \gamma\gamma$ also appear at the leading order. The

NLO computation involves two kinds of matrix elements.

- Virtual diagrams with loops which contribute through their interference with the LO diagrams (see fig.(2)).
- Real emission diagrams with an additional parton in the final state (see fig.(3)).

Both the virtual and real corrections have been evaluated with 5 quark flavors and in the limit of vanishing of quark masses. The n-point tensor integrals appearing from integration over loop-momenta were simplified using Passarino-Veltman reduction and computation was carried with dimensional regularization using $n = 4 + \epsilon$, and divergences were subtracted or factorized in $\overline{MS}$ scheme.

Photons not only arise directly in a parton subprocess but also through fragmentation of a parton into a photon and a jet of hadrons collinear to it. This fragmentation is a non-perturbative phenomenon. A parton level computation involving only direct photons without including fragmentation photons is plagued with QED collinear singularities. It is evident from the SM Feynman diagrams. This singularity can be absorbed into fragmentation functions describing probability of a parton fragmenting into a photon in much the same way as initial state collinear singularities are absorbed in parton distribution functions. However, fragmentation functions are not known to a good accuracy. An alternative is to avoid these fragmentation functions and simultaneously suppress final state QED singularity by using the *smooth cone isolation* criterion advocated by Frixione [23].

Smooth cone isolation: The aim of this isolation criterion is to suppress the final state QED collinear singularities and at the same time also remove the fragmentation photons in an infrared safe manner. Let the z-axis coincide with the proton-proton collision line and θ and ϕ denote the polar and azimuthal angles respectively. It is, however, more convenient to use the pseudo-rapidity in the context of hadron colliders, as they are additive under boosts. The fragmentation photons are embedded in hadronic jets and the prescription to isolate a photon from hadronic activity is to

draw concentric circles around it in $\eta - \phi$ plane with the largest circle having a fixed radius R_0, which will be taken as $R_0 = 0.4$, and demand that the sum of hadronic transverse energy in any circle of radius $R < R_0$ be less than some specified amount $H(R)$. Thus as we move closer to the photon lesser hadronic energy is allowed in its neighborhood. In order that this criterion does not disturb cancellation of infrared singularities $H(R)$ is restricted to have the limit $H(R \to 0) = 0$. Here we would use the following choice for $H(R)$

$$H(R) = E_T^{iso} \left(\frac{1 - \cos R}{1 - \cos R_0} \right)^n , \tag{5}$$

where E_T^{iso} is a fixed energy. In this paper, for our analysis, $n = 2$ and $E_T^{iso} = 15$ GeV would be default choices.

The paper is organized as follows. In section-2, we outline the next-to-leading order computation in the two cut off phase space slicing method and present all the analytical results that go into our Monte Carlo code with the exception of $2 \to 3$ subprocess matrix elements [5]. In section-3, the numerical results and discussion on various kinematical distributions are presented. Finally we conclude in the section-4.

2 Outline of computation

2.1 Leading order processes

A parton level $2 \to 2$ process at the leading order is of the generic form

$$a(p_1) + b(p_2) \to \gamma(p_3) + \gamma(p_4). \tag{6}$$

[5] These can be obtained from us on request

where a and b are either quark and anti-quark or gluons. The exact matrix elements in $n = 4 + \epsilon$ dimensions for $q\overline{q}$ and gg initiated subprocesses are

$$\overline{|M^{(0)}|^2}_{q\overline{q},sm} = \frac{e_q^4}{N}\left[\frac{u}{t}+\frac{t}{u}+\epsilon\left(1+\frac{u}{t}+\frac{t}{u}\right)+\frac{\epsilon^2}{4}\left(2+\frac{u}{t}+\frac{t}{u}\right)\right] \tag{7}$$

$$\overline{|M^{(0)}|^2}_{q\overline{q},int} = -\kappa^2\mathcal{R}e\mathcal{D}(s)\ \frac{e_q^2}{8N}\left[4\left(t^2+u^2\right)+\epsilon\left(3t^2+3u^2+2ut\right)\right] \tag{8}$$

$$\overline{|M^{(0)}|^2}_{q\overline{q},gr} = \frac{\kappa^4|\mathcal{D}(s)|^2}{16N}\left[ut^3+tu^3+\frac{\epsilon}{4}\left(3tu^3+3t^3u+2u^2t^2\right)\right], \tag{9}$$

$$\begin{aligned}\overline{|M^{(0)}|^2}_{gg,gr} = \frac{\kappa^4|\mathcal{D}(s)|^2}{N^2-1}\Big[&\frac{81}{128(3+\epsilon)^2}s^4+\frac{27}{64(3+\epsilon)}s^2\left(u^2+14tu+t^2\right)\\ &+\frac{5}{2(2+\epsilon)^2}s^2tu-\frac{1}{16(2+\epsilon)}s^2\left(7u^2+94tu+7t^2\right)\\ &+\frac{1}{128}\left(9t^4+28t^3u+54t^2u^2+28tu^3+9u^4\right)\Big]\end{aligned} \tag{10}$$

where $sm,\ gr,\ int$ represent contributions from SM, gravity, and interference of SM with gravity induced process respectively, s, t, u are the usual Mandelstam invariants, e_q is the charge of a quark or anti-quark and κ is the coupling of gravity to SM fields. The bar over the symbol M represents that the matrix elements have been averaged over initial helicities and color, and summed over the final ones. A factor of $1/2$ has been included for identical final state photons. This expression has been evaluated for quarks with N and gluons with N^2-1 color degrees of freedom.

2.2 Virtual process

The order α_s corrections to leading order process come from interference between Born graphs and virtual graphs. It is to be noted that the virtual contribution here does not contain UV singularities. The reason lies in the facts that (i) electromagnetic coupling α does not receive any QCD corrections, (ii) and that the gravitons couple to the energy momentum tensor of SM fields which is a conserved quantity and does not get renormalized. The Feynman diagrams with external leg corrections are not shown as these vanish in the dimensional regularization in the massless limit. We

give below the order α_s squared matrix element coming from virtual processes. The SM contribution is found to be

$$\overline{|M^V|^2}_{q\overline{q},sm} = a_s(\mu_R^2) f(\epsilon,\mu_R^2,s) C_F \left[\Upsilon(\epsilon)\ \overline{|M^{(0)}|^2}_{q\overline{q},sm} + 2\frac{e_q^4}{N} \left\{ (4\zeta(2)-7)\frac{u}{t} + \left(2+3\frac{u}{t}\right)\ln\frac{-t}{s} + \left(2+\frac{u}{t}+2\frac{t}{u}\right)\ln^2\frac{-t}{s} + t \leftrightarrow u \right\} \right], \quad (11)$$

the interference of SM with the gravity mediated processes are

$$\begin{aligned} \overline{|M^V|^2}_{q\overline{q},int} = a_s(\mu_R^2) f(\epsilon,\mu_R^2,s) C_F \Bigg[& \Upsilon(\epsilon)\,\overline{|M^{(0)}|^2}_{q\overline{q},int} + \kappa^2 \mathcal{R}e\mathcal{D}(s)\frac{e_q^2}{2N} \Big\{ (17-8\zeta(2))t^2 \\ & -(2tu+3u^2)\ln\frac{-t}{s} - \left(2tu+2t^2+u^2\right)\ln^2\frac{-t}{s} + t \leftrightarrow u \Big\} \\ & -\kappa^2 \pi \mathcal{I}m\mathcal{D}(s)\frac{e_q^2}{2N} \left\{ 3t^2+2tu+2(t^2+2tu+2u^2)\ln\frac{-u}{s} + t \leftrightarrow u \right\} \Bigg] \quad (12) \end{aligned}$$

$$\begin{aligned} \overline{|M^V|^2}_{gg,int} = a_s(\mu_R^2)\, e_q^2\kappa^2\, \frac{1}{N^2-1} \Bigg[& s\, \mathcal{R}e\mathcal{D}(s) \left\{ u^2 + (2tu+t^2)\ln\frac{-u}{s} \right. \\ & \left. + \left(u^2+\frac{1}{2}t^2+tu\right)\ln^2\frac{-u}{s} \right\} + s\,\pi\mathcal{I}m\mathcal{D}(s) \left\{ u^2+2tu \right. \\ & \left. +(2u^2+2tu+t^2)\ln\frac{-u}{s} \right\} + t \leftrightarrow u \Bigg], \quad (13) \end{aligned}$$

and the pure gravity contributions are

$$\overline{|M^V|^2}_{q\overline{q},gr} = a_s(\mu_R^2) f(\epsilon,\mu_R^2,s) C_F \left[\Upsilon(\epsilon)\,\overline{|M^{(0)}|^2}_{q\overline{q},gr} + 4(2\zeta(2)-5)\overline{|M^{(0)}|^2}_{q\overline{q},gr} \right] \quad (14)$$

$$\begin{aligned} \overline{|M^V|^2}_{gg,gr} = & a_s(\mu_R^2) f(\epsilon,\mu_R^2,s) C_A \left[\left\{ -\frac{16}{\epsilon^2} + \frac{4}{C_A\epsilon}\left(\frac{11}{3}C_A - \frac{4}{3}n_f T_f\right) \right\} \overline{|M^{(0)}|^2}_{gg,gr} \right. \\ & \left. + \frac{1}{9}\left(72\zeta(2) + 70\frac{n_f T_f}{C_A} - 203\right)\overline{|M^{(0)}|^2}_{gg,gr} \right] \quad (15) \end{aligned}$$

where

$$\Upsilon(\epsilon) = -\frac{16}{\epsilon^2} + \frac{12}{\epsilon}, \qquad f(\epsilon,\mu_R^2,s) = \frac{\Gamma\left(1+\frac{\epsilon}{2}\right)}{\Gamma(1+\epsilon)}\left(\frac{s}{4\pi\mu_R^2}\right)^{\frac{\epsilon}{2}} \quad (16)$$

Here μ_R^2 is the scale at which the theory is renormalized ; $a_s(\mu_R^2) = g_s(\mu_R^2)^2/16\pi^2$ is the strong running coupling constant. Our results for the SM are in agreement with the literature [20]. The poles in ϵ arise from loop integrals and correspond to the soft and collinear divergences. Configurations in which a virtual gluon momentum goes to zero give soft singularities while collinear singularities arise when two massless partons become collinear to each other. As the soft divergences cancel completely in any observable, the ϵ poles of order-2, get canceled when real emission contributions are included. This cancellation will be shown in what follows.

2.3 Real emission process

A next-to-leading order $2 \to 3$ parton level process for production of photon pairs is of the following generic form

$$a(p_1) + b(p_2) \to \gamma(p_3) + \gamma(p_4) + c(p_5). \tag{17}$$

where a,b and c are massless partons. In fig.(3) all gravity mediated $2 \to 3$ Feynman diagrams are given. Depending on the initial state partons, the final state may have a quark or anti-quark or a gluon. To obtain an inclusive cross-section the final state parton will be integrated over the phase-space. The $2 \to 3$ matrix elements when integrated over the phase-space give soft and collinear singularities. These singularities are regulated using dimensional regularization with $n = 4 + \epsilon$ and appear as poles in ϵ. These singularities arise when the final state gluon becomes soft (a soft fermion does not give any soft divergences) or when the final state massless parton becomes collinear to an initial state massless parton. As was mentioned in the introduction a Monte Carlo approach allows for an easy implementation of experimental cuts on the final state photons and smooth-cone isolation criterion. This is achieved by using the semi-numerical two cutoff phase space slicing method. This method introduces two small dimensionless parameters δ_s and δ_c to deal with soft and collinear QCD singularities. δ_s divides the phase-space into *soft* and *hard* regions. The part of phase-space where the energy of the gluon in the centre of mass frame of incom-

ing parton is less than $\delta_s\sqrt{s}/2$ is defined as $soft$ and the region complementary to it is $hard$. For small values of δ_s the matrix elements can be simplified and integrated over the soft region to give a δ_s dependent, order α_s, 2-body contribution $d\sigma_S(\delta_s, \epsilon)$. This contains the poles in ϵ arising from the soft singularities. The hard region can be further divided into collinear and non-collinear regions using another small dimensionless slicing parameter δ_c. The part of phase-space in which the final state parton is collinear to the incoming parton is defined as collinear region and gives an order α_s contribution $d\sigma_{HC}(\delta_s, \delta_c, \epsilon)$. This contains the collinear singularities. The hard non-collinear 3-body contribution denoted by $d\sigma_{\overline{HC}}(\delta_s, \delta_s)$ is free of any singularities and can be evaluated numerically using Monte Carlo integration. The collinear singularities appearing in $d\sigma_{HC}(\delta_s, \delta_c, \epsilon)$ will be removed by mass factorization in $\overline{MS}$ scheme by adding counter terms to give $d\sigma_{HC+CT}(\delta_s, \delta_c, \epsilon)$. In the following subsections it will be shown that the 2-body contribution $d\sigma_V(\epsilon) + d\sigma_S(\delta_s, \delta_c, \epsilon) + d\sigma_{HC+CT}(\delta_s, \delta_c, \epsilon)$ is free of poles in ϵ. Although individually the 2-body and 3-body contributions depend on the slicing parameters which were introduced artificially in the problem, the sum should be independent of these parameters. In what follows we will show that this sum is independent of δ_s and δ_c for a fairly wide rage of these parameters.

2.3.1 Soft

In the soft gluon limit the $2 \to 3$ amplitude factorizes into Born matrix element and a term containing eikonal currents. These eikonal currents reveal the singularities when integrated over the soft part of phase space.

$$d\hat{\sigma}_S = a_s(\mu_R^2) f(\epsilon, \mu_R^2, s) \Big(C_F \, d\hat{\sigma}^0_{q\overline{q}}(\epsilon) + C_A \, d\hat{\sigma}^0_{gg}(\epsilon) \Big) \left[\frac{16}{\epsilon^2} + \frac{16}{\epsilon} \ln \delta_s + 8 \ln^2 \delta_s \right] \tag{18}$$

The symbol $\hat{\sigma}$ is used to indicate that the cross-section is at parton level. The terms linear and higher order in δ_s have been dropped. Note that the $1/\epsilon^2$ pole cancels with the virtual contribution. However the pole $1/\epsilon$ with coefficient $\ln \delta_s$ still remains uncanceled and later it will be seen that this pole also cancels.

2.3.2 Collinear

Complementary to the soft region discussed above is the hard region. In this region collinear singularities arise when the final state massless parton (quark, anti-quark or gluon) is collinear to the initial state parton. Let z denote the momentum fraction of the incoming parton carried by the parton entering into hard scattering. An initial state quark can split into a quark (and a gluon) or into a gluon (and a quark) which enter into the hard scattering and involve P_{qq} and P_{gq} splitting functions. Similarly an initial state gluon gives P_{gg} and P_{qg} splitting functions. If the energy of a final state gluon is greater than $\delta_s\sqrt{s}/2$ in the rest frame of incoming partons it is defined as a hard gluon. Thus a gluon is hard if $0 \leq z \leq 1-\delta_s$ for P_{qq} and P_{gg} splittings. As a soft quark does not give any soft singularities, $0 \leq z \leq 1$ for P_{gq} and P_{gq} splittings. As already discussed above, in the collinear limit matrix elements simplify and can be integrated easily in $n = 4+\epsilon$ dimensions over the collinear region. For photon pair

production the hard collinear contribution takes the following form

$$
\begin{aligned}
d\sigma_{HC} \;=\; & \frac{a_s(\mu_R^2)}{\epsilon} dx_1 dx_2 f(\epsilon, \mu_R^2, s) \\
& \times \Bigg[d\hat{\sigma}_0^{q\overline{q}}(x_1, x_2, \epsilon) \Big\{ \int_{x_2}^{1-\delta_s} \frac{dz}{z} \mathcal{H}(z, \epsilon, \delta_c) P_{qq}(z, \epsilon) \sum_i f_{q_i}(x_1) f_{\overline{q}_i}(x_2/z) \\
& + \int_{x_1}^{1-\delta_s} \frac{dz}{z} \mathcal{H}(z, \epsilon, \delta_c) P_{qq}(z, \epsilon) \sum_i f_{q_i}(x_1/z) f_{\overline{q}_i}(x_2) + x_1 \leftrightarrow x_2 \Big\}_{q\overline{q}} \\
& + d\hat{\sigma}_0^{q\overline{q}}(x_1, x_2, \epsilon) \Big\{ \int_{x_2}^{1} \frac{dz}{z} \mathcal{H}(z, \epsilon, \delta_c) P_{qg}(z, \epsilon) \sum_i f_{q_i}(x_1) f_g(x_2/z) \\
& + \int_{x_2}^{1} \frac{dz}{z} \mathcal{H}(z, \epsilon, \delta_c) P_{qg}(z, \epsilon) \sum_i f_{\overline{q}_i}(x_1) f_g(x_2/z) + x_1 \leftrightarrow x_2 \Big\}_{qg} \\
& + d\hat{\sigma}_0^{gg}(x_1, x_2, \epsilon) \Big\{ \int_{x_2}^{1-\delta_s} \frac{dz}{z} \mathcal{H}(z, \epsilon, \delta_c) P_{gg}(z, \epsilon) \sum_i f_g(x_1) f_g(x_2/z) + x_1 \leftrightarrow x_2 \Big\}_{gg} \\
& + d\hat{\sigma}_0^{gg}(x_1, x_2, \epsilon) \Big\{ \int_{x_2}^{1-\delta_s} \frac{dz}{z} \mathcal{H}(z, \epsilon, \delta_c) P_{gq}(z, \epsilon) \sum_i f_g(x_1) f_{q_i}(x_2/z) \\
& + \int_{x_2}^{1-\delta_s} \frac{dz}{z} \mathcal{H}(z, \epsilon, \delta_c) P_{gq}(z, \epsilon) \sum_i f_g(x_1) f_{\overline{q}_i}(x_2/z) + x_1 \leftrightarrow x_2 \Big\}_{qg} \Bigg]
\end{aligned}
\tag{19}
$$

where x_1, x_2 are momentum fraction of incoming parton momenta $P_{ij}(z, \epsilon)$ are splitting functions in $4 + \epsilon$ dimensions, and

$$
\mathcal{H}(z, \epsilon, \delta_c) = \left(\delta_c \frac{1 - z}{z} \right)^{\epsilon/2}. \tag{20}
$$

The collinear singularities can be removed by the method of mass factorization. To this effect, counter terms to cancel these singularities in $\overline{MS}$ scheme are obtained by introducing in the leading order cross-section

$$
\begin{aligned}
d\sigma_0 \;=\; & dx_1 dx_2 \Big(d\hat{\sigma}_0^{q\overline{q}}(x_1, x_2, \epsilon) \sum_i \Big[f_{q_i}(x_1) f_{\overline{q}_i}(x_2) + f_{\overline{q}_i}(x_1) f_{q_i}(x_2) \Big] \\
& + d\hat{\sigma}_0^{gg}(x_1, x_2, \epsilon) f_g(x_1) f_g(x_2) \Big)
\end{aligned}
\tag{21}
$$

the following factorization scale dependent parton distribution functions in the $\overline{MS}$ scheme.

$$f_q(x) = f_q(x,\mu_F) - \frac{a_s(\mu_R^2)}{\epsilon}\left(\frac{\mu_F^2}{\mu_R^2}\right)^{\frac{\epsilon}{2}}\int_x^1 \frac{dz}{z}\Big[P_{qq}(z)f_q(x/z) + P_{qg}(z)f_g(x/z)\Big]$$

$$f_g(x) = f_g(x,\mu_F) - \frac{a_s(\mu_R^2)}{\epsilon}\left(\frac{\mu_F^2}{\mu_R^2}\right)^{\frac{\epsilon}{2}}\int_x^1 \frac{dz}{z}\Big[P_{gg}(z)f_g(x/z) + P_{gq}(z)\big(f_q(x/z) + f_{\overline{q}}(x/z)\big)\Big] \tag{22}$$

Note that the upper limits on the integrals are 1 for all the splittings. Substituting these distribution functions in $d\sigma_0$ an adding to σ_{HC} the following order a_s term is obtained.

$$\begin{aligned} d\sigma_{HC+CT} = a_s(\mu_R^2)dx_1dx_2f(\epsilon,\mu_R^2,s)\Bigg[& d{\sigma_0}^{q\overline{q}}(\epsilon)\sum_i f_{\overline{q}_i}(x_1,\mu_F)\Bigg\{\frac{1}{2}\tilde{f}_{q_i}(x_2,\mu_F) \\ & +\Big(f_{q_i}(x_2,\mu_F)A_{q\to q+g} + f_g(x_2,\mu_F)A_{g\to q+\overline{q}}\Big)\Big(-\frac{1}{\epsilon}+\frac{1}{2}\ln\frac{s}{\mu_F^2}\Big)\Bigg\} \\ & +d{\sigma_0}^{gg}(\epsilon)f_g(x_1,\mu_F)\Bigg\{\frac{1}{2}\tilde{f}_g(x_2,\mu_F) + \Big(f_g(x_2,\mu_F)A_{g\to g+g} \\ & +\sum_i f_{q_i}(x_2,\mu_F)A_{q\to g+q}\Big)\Big(-\frac{1}{\epsilon}+\frac{1}{2}\ln\frac{s}{\mu_F^2}\Big)\Bigg\}\Bigg] + (q\leftrightarrow\overline{q}, x_1\leftrightarrow x_2) \end{aligned} \tag{23}$$

The function $A_{a\to b+c}$ result from the mismatch in the integral limits on $z-$integrals in $d\sigma_{HC}$ and counter term and can be easily evaluated using the definition of *plus*-prescription.

$$\begin{aligned} A_{q\to q+g} &= 4C_F\left(2\ln\delta_s + \frac{3}{2}\right), & A_{q\to g+q} &= 0. \\ A_{g\to g+g} &= \frac{22}{3}C_A - \frac{4}{3}n_f + 8C_A\ln\delta_s, & A_{g\to q+\overline{q}} &= 0, \end{aligned} \tag{24}$$

The function $\tilde{f}_{q,g}$ are defined by

$$\begin{aligned}
\tilde{f}_q(x,\mu_F) &= \int_x^{1-\delta_s} \frac{dz}{z} f_q\left(\frac{x}{z},\mu_F\right)\tilde{P}_{qq}(z) + \int_x^1 \frac{dz}{z} f_g\left(\frac{x}{z},\mu_F\right)\tilde{P}_{qg}(z) \\
\tilde{f}_g(x,\mu_F) &= \int_x^{1-\delta_s} \frac{dz}{z} f_q\left(\frac{x}{z},\mu_F\right)\tilde{P}_{gq}(z) + \int_x^1 \frac{dz}{z} f_g\left(\frac{x}{z},\mu_F\right)\tilde{P}_{gg}(z) \qquad (25)
\end{aligned}$$

with

$$\tilde{P}_{ij}(z) = P_{ij}(z)\ln\left(\delta_c \frac{1-z}{z}\frac{s}{\mu_F^2}\right) - P'_{ij}(z) \qquad (26)$$

The P' is the order ϵ part of $P_{ij}(z,\epsilon)$.

After mass factorization the poles still remain and do not cancel completely in $d\sigma_{HC+CT}$ and these cancel with the uncanceled simple poles in virtual and soft contributions. The contribution $d\sigma_{HC+CT} + d\sigma_S + d\sigma_V$ is an order a_s 2-body contribution free of any singularities and can be evaluated numerically using Monte Carlo integration with the experimental cuts on the final state photons. This, however depends on the choice of arbitrary small parameters δ_s and δ_c used for slicing of phase space. The 3-body hard non collinear contribution also depends on slicing parameters and is free of any singularities and can be evaluated numerically. The sum of 2-body and 3-body contribution should be independent of the δ_s and δ_c.

3 Numerical Results

In this section various kinematical distributions for production of isolated direct photon pairs are presented to next-to-leading order accuracy in QCD both in the ADD and RS scenarios. Both for the SM background and the SM+ADD and SM+RS signals the following distributions are presented:

1. Invariant mass (Q) distribution of the di-photon system
2. Transverse momentum (Q_T) distribution of the photon pair
3. Angular distribution $\cos\theta^*$ of the photons

4. Rapidity (Y) distribution of the di-photon system.

5. Rapidity y^γ distribution of photon

We impose the same kinematical cuts on the two photons in our study which are used by ATLAS and CMS collaborations [24,25]: (i) $p_T^\gamma > 40\,(25)$ GeV for the harder (softer) photons, (ii) rapidity $|y_\gamma| < 2.5$ for each of the photons. (iii) The minimum separation between the two photons in the $y-\phi$ plane is taken to be $R_{\gamma\gamma} = 0.4$. As this study does not include poorly known fragmentation functions, the final state QED singularity is suppressed using the smooth cone isolation discussed in eqn.(5). In what follows $E_T^{iso} = 15$ GeV and $n = 2$ with $R_0 = 0.4$ would be our default choices. This choice allows a maximum of hadronic transverse energy equal to 15 GeV in a cone of radius 0.4 in $\eta-\phi$ plane around a photon. As parton in the final state in our NLO computation is a crude approximation to the jet of hadrons detected in the detectors, the dependence of results on the choice of the parameters entering into isolation criterion needs to be studied and it has been observed in [17] to be small. For our leading order analysis we have used CTEQ6L, and for NLO analysis CTEQ6M [26] parton density sets respectively with $n_f = 5$ light quark flavours, and the corresponding two loop strong running coupling constant $\alpha_s(M_Z) = 0.118$. The fine structure constant is taken to be $\alpha(M_W) = 1/128$. Unless mentioned otherwise we have set the renormalization and the factorization scales to $\mu_R = \mu_F = Q$ in all the distributions.

Before proceeding further we present the stability of the sum of 2-body and 3-body contributions against the variation of the slicing parameters δ_s and δ_c. In fig(4) and fig(5) the individual 2-body and 3-body order α_s contributions and their sum are presented in invariant mass distribution in the SM and SM+ADD respectively as a function of δ_s with δ_c fixed at 10^{-5}. From these figures it is clear that the sum is fairly stable against the variation of slicing parameters; this serves as a check on the numerical implementation of the phase space slicing in our numerical code. Fig(9) provides the corresponding test for the case of the RS model. For all further analysis, we choose $\delta_s = 10^{-3}$ and $\delta_c = 10^{-5}$. As a further test we compared our SM results

with those in [10]. Our SM results are in good agreement with [10] when the isolation criterion used there is used in our code. This gives a further confidence in our code.

3.1 ADD model distributions

In this section, we study various kinematic distributions in the ADD model using our NLO results. First, we present our results for the invariant mass distribution. In fig.(6a), we plot LO and NLO contributions to the signal (SM+ADD) and the SM background against Q between 300 GeV and 1 TeV. We choose the fundamental scale $M_S = 2$ TeV and the number of extra dimensions $d = 3$. As we discussed in the introduction, we do not consider the gluon-gluon fusion process through quark loop at LO as its contribution is significant only at small Q.

For the above choice of parameters the signal starts deviating from the SM background around $Q = 500$ GeV. The value of Q at which the deviation occurs depends very much on the choice of the parameters, namely the scale M_S, d and the cut-off scale Λ for the summation of the KK modes. In fig.(6b), we show how the invariant mass distribution depends on the choice of the fundamental scale M_S when $d = 3$. As expected smaller the M_S, the larger the deviation one observes. The dependence on the number of extra dimensions d is presented in fig.6c for $d = 3 - 6$ keeping $M_S = 2$ TeV fixed. We find that the ADD contribution decreases with increase in d. In fig.(6d), we present the cut-off scale Λ dependence for $\Lambda = 0.6 M_S$ to M_S. For lower values of cut-off scale, the number of KK modes available are less and the signal will decrease with decrease in Λ as shown in the figure. In the following, we choose $M_S = 2$ TeV, $d = 3$ and $\Lambda = M_S$. For the rest of the kinematic distributions that we have considered, to reduce the SM background and to enhance the signal, we integrate over Q in the range $600 < Q < 1100$ GeV.

The rapidity of the photon pair is defined by

$$Y = \frac{1}{2} \ln \left(\frac{P_1.q}{P_2.q} \right) \tag{27}$$

where P_1, P_2 are the momenta of incoming hadrons and $q = p_3 + p_4$. In the left panel

of fig.(7), we show the production cross section as a function of Y between -2.0 and 2.0 after integrating over Q in the region $600 < Q < 1100$ GeV where the ADD model shows significant contribution over the SM background. From the left panel of this figure, we observe that the signal exceeds the background by more than an order of magnitude at the central rapidity region $Y = 0$.

The transverse momentum of the photon pair is defined by $Q_T = \sqrt{q_x^2 + q_y^2}$. At LO, the photon pairs will have zero Q_T as incoming partons have no transverse momentum, and hence Q_T distribution will be proportional to $\delta(Q_T)$. However, at NLO, the photon pairs will be accompanied by a quark (anti-quark) or a gluon in the final state resulting in a non-zero Q_T. The numerical results for the Q_T distribution is presented in the right panel of fig.(7).

The rapidity of a photon is given by

$$y^\gamma = \frac{1}{2} \ \ln\left(\frac{E + p_z}{E - p_z}\right) \tag{28}$$

where E and p_z are its energy and the longitudinal momentum respectively. In fig.(8), the left panel shows the rapidity distribution of the photons as a function of y^γ in the region $-2.0 < y^\gamma < 2.0$. The SM cross sections both at LO and NLO level do not show significant dependence on y^γ unlike contribution from the ADD model. We also find that the QCD corrections are large for the signal as compared to the SM background.

For the angular distribution of the photons, we define

$$\cos\theta^* = \frac{P_1.(p_3 - p_4)}{P_1.(p_3 + p_4)} \tag{29}$$

Since gravitons are spin-2 particles, the angular dependence of the cross section in ADD model will be different from SM. It is shown in the right panel of fig.(8). Hence these distributions have the advantage of distinguishing the signal, qualitatively, from the background.

3.2 RS model distributions

In this section we present the kinematic distributions of the photon pairs in the RS model at the LHC to order α_s. Unlike the ADD model wherein the spectrum of the

KK modes is uniform and almost continuous, the spectrum in the RS model is quite non-uniform and contains heavy resonances. They can be probed via their resonance decays at large values of Q. In fig.(11), we present the invariant mass distribution of the di-photon in the RS model with the following choice of parameters: (i) the mass of the first RS mode is $M_1 = 1.5$ TeV and (ii) the effective coupling between the RS modes and the SM fields is $c_0 = 0.01$. This choice is consistent with the bounds obtained from the Tevatron [15]. The RS modes being heavy show up as resonances in the invariant mass distribution which can be seen in the left panel of the figure. In the right panel, we have plotted the rapidity distribution of the photon pairs (see eqn.(27)) after integrating the invariant mass of the photon pairs around the first resonance i.e. in the range $1100 < Q < 1600$ GeV. We find that the signal has maximum contribution at the central rapidity (Y=0) and is differing from the SM background by an order of magnitude. The NLO QCD corrections enhance the signal and the background. Even though, the resonance pattern in the high Q region can point to new physics, identification of the spin of the resonance will be very important to discriminate between the various new physics scenarios. It is well known that spin information of these resonances will be reflected in the angular distribution and we study them in the following.

In fig.(12), rapidity y^γ of the photons is plotted $|y^\gamma| \leq 2.0$ both in the SM and in SM+ADD to order α_s. This distribution is obtained after integrating over the invariant mass of the photon pairs in the range $1100 \leq Q \leq 1600$ GeV where RS resonance shows up. The SM cross sections show very little variation with respect to y^γ while the signal peaks at the central rapidity. The cosine of the angle (see eqn.(29)) between the final state photon and one of the incoming hadrons in the c.o.m. frame of the final state photons is plotted in the fig.(12) in the range $|\cos\theta^*| \leq 0.95$. Again, we have restricted our $1100 \leq Q \leq 1600$ GeV as in the case of y^γ distribution. The distribution coming from the SM has a minimum for the photons in the transverse direction and becomes large for the photons close to the beam direction. However, in the RS model,

the signal shows an oscillating behavior and differs by more than an order of magnitude for the photons in the transverse direction. This is the feature unique to new physics scenarios where spin-2 objects decay to photon pairs. We find our QCD corrections enhance the cross sections. We present the Q_T distribution which is non-zero only at order α_s. This is obtained after integrating Q in the range $1100 \leq Q \leq 1600$ GeV. The numerical results are shown in fig.(13). We find that the signal has a large enhancement over the SM background for the entire range of Q_T considered i.e. from 100 GeV to 900 GeV.

3.3 Scale variations

In this section, we discuss the impact of NLO QCD corrections to various distributions. The uncertainity in LO computation of observables in the hadron colliders originates from two important sources, namely, the missing higher order radiative corrections and the choice of factorisation and renormalisation scales. The former enters through parton density sets and the latter through the renormalised parameters such as running coupling constant α_s of the theory. The radiative corrections coming from QCD in our case enhance both SM as well as ADD and RS distributions. Hence, the K-factor ($K = \sigma^{NLO}/\sigma^{LO}$), that quantifies these effects is always positive for the cases we studied in this paper. It is clear from the plots that the K-factor is different for different distributions and also within a given distribution, it varies with the kinematical variable, say Q or Y etc. More importantly, the numerical value of K depends very much on the kinematical cuts imposed on each distribution. We find that the K factors of the distributions reported in the paper are not large and hence our NLO results are stable under perturbation and reliable for further study. Observables are expected to be independent of renormalisation and factorisation scales, thanks to renormalisation group invariance. However, any truncated perturbative expansion does depend on the choice of these scales. This is expected to improve if higher order corrections are included in the perturbative expansion. Indeed, our NLO results of these distributions show significant improvement on the factorisation scale uncer-

tainity entering through parton density sets at LO level. In order that the perturbative expansion does not break down these scales should be chosen close to the scale in the problem such as Q or Q_T. In the fig.(14) we show the effect of variation of μ_F between $Q/2$ and $3Q/2$. We studied this variation for Y and $\cos\theta^*$ distributions in the ADD model. A similar analysis has been done for the RS model as well which is shown in fig.(15) Here, we have integrated the invariant mass around the first resonance region $1100 \leq Q \leq 1600$ GeV.

4 Conclusions

In this paper, we have presented full next to leading order QCD corrections to production of direct photon pairs at hadron colliders in the context of extra-dimension scenarios namely ADD and RS models. Both in ADD and RS models, photon pairs can be produced in a collision of partons through virtual exchange of KK gravitons. These give appreciable deviations to production rates predicted in the SM due to large multiplicity of KK modes in the ADD and warp factor in the RS model. Only the spin-2 gravitons are included in our analysis and they show distinct features in the angular distributions of photon pairs. Photon pairs at hadron colliders often provide a clean channel to probe these physics beyond the SM. In this study, only direct photons have been considered and the fragmentation photons are removed by the method of smooth cone isolation. The isolation used also removes final state QED singularities. The leading order contributions to production rate resulting from quark and anti quark as well as gluon initiated processes depend very much on the factorisation scale through the parton distribution functions giving significant theory uncertainity. In order to bring down this uncertainity, we have systematically included all order α_s contributions to the process. This includes all virtual and real emission processes to order α_s both in SM as well as in ADD and RS models. To obtain various kinematic distributions of the final state photons, we have used phase space slicing method to deal with all the soft and collinear singularities and the resulting finite pieces are inte-

grated with the appropriate kinematical cuts using a Monte Carlo program. We have made several test on our NLO code by showing the independence of the results on the slicing parameters and also comparing with the known NLO corrected SM results available in the literature. Our numerical results including the NLO corrections show significant enhancement over the LO predictions in all the distributions presented. The enhancement varies with the distributions. We have estimated them through the K-factor which quantifies the reliability of the perturbative expansion. We find the K-factor is moderate for all the distributions and hence the results present here are stable under perturbation. We have also shown the impact of α_s corrected results on the scale uncertainity. We find that the factorisation scale dependence gets reduced considerably when α_s contributions are included.

Acknowledgments: MCK would like to thank CSIR, New Delhi for financial support. The work of VR and AT has been partially supported by funds made available to the Regional Centre for Accelerator-based Particle Physics (RECAPP) by the Department of Atomic Energy, Govt. of India. AT and VR would like to thank the cluster computing facility at Harish-Chandra Research Institute where part of computational work for this study was carried out.

References

[1] N. Arkani-Hamed, S. Dimopoulos and G. R. Dvali, Phys. Lett. B **429** (1998) 263; I. Antoniadis, N. Arkani-Hamed, S. Dimopoulos and G. R. Dvali, Phys. Lett. B **436** (1998) 257.

[2] L. Randall and R. Sundrum, Phys. Rev. Lett. **83** (1999) 3370; W.D. Goldberger and M.B. Wise, Phys. Rev. Lett. **83** (1999) 4922.

[3] C. D. Hoyle *et. al*, *Phys. Rev.* **D70** (2004) 042004.

[4] T. Han, J. D. Lykken and R. J. Zhang, Phys. Rev. D **59** (1999) 105006.

[5] G. F. Giudice, R. Rattazzi and J. D. Wells, *Nucl. Phys.* **B544** (1999) 3.

[6] E. A. Mirabelli, M. Perelstein, M. E. Peskin Phys. Rev. Lett. 82 (1999) 2236.

[7] Prakash Mathews, Sreerup Raychaudhuri, K. Sridhar Phys. Lett. B450 (1999) 343; Prakash Mathews, Sreerup Raychaudhuri, K. Sridhar Phys. Lett. B455 (1999) 115; Prakash Mathews, Sreerup Raychaudhuri, K. Sridhar JHEP 0007 (2000) 008.

[8] W.D. Goldberger and M.B. Wise, *Phys. Rev. Lett.* **83** (1999) 4922; *ibid Phys.Lett.* **B475** (2000) 275.

[9] H. Davoudiasl, J.L. Hewett and T.G. Rizzo, *Phys. Rev. Lett* **84** (2000) 2080; *ibid. Phys. Rev.* **D63** (2001) 075004.

[10] Z. Bern, L. J. Dixon and C. Schmidt, Phys. Rev. D **66** (2002) 074018 [arXiv:hep-ph/0206194].

[11] E.L. Berger, E. Braaten and R.D. Field, Nucl. Phys. B **239**, 52 (1984); P. Aurenche, A. Douiri, R. Baier, M. Fontannaz and D. Schiff, Z. Phys. C **29**, 459 (1985); B. Bailey, J.F. Owens and J. Ohnemus, Phys. Rev. D **46**, 2018 (1992); B. Bailey and J.F. Owens, Phys. Rev. D **47**, 2735 (1993); B. Bailey and D. Graudenz, Phys. Rev. D **49**, 1486 (1994) [arXiv:hep-ph/9307368]; C. Balazs, E.L. Berger, S. Mrenna and C.-P. Yuan, Phys. Rev. D **57**, 6934 (1998) [arXiv:hep-ph/9712471]; C. Balazs and C.-P. Yuan, Phys. Rev. D **59**, 114007 (1999) [Erratum-ibid. D **63**, 059902 (1999)] [arXiv:hep-ph/9810319]; T. Binoth, J.P. Guillet, E. Pilon and M. Werlen, Phys. Rev. D **63**, 114016 (2001) [arXiv:hep-ph/0012191]; T. Binoth, arXiv:hep-ph/0005194. T. Binoth, J.P. Guillet, E. Pilon and M. Werlen, Eur. Phys. J. C **16**, 311 (2000) [arXiv:hep-ph/9911340].

[12] O. J. P. Eboli, T. Han, M. B. Magro and P. G. Mercadante, Phys. Rev. D **61** (2000) 094007 [arXiv:hep-ph/9908358]; K. m. Cheung and G. L. Landsberg, Phys. Rev. D **62** (2000) 076003 [arXiv:hep-ph/9909218]; M. Luo, L. Wang and G. Zhu, Phys. Lett. B **672** (2009) 65 [arXiv:0812.0866 [hep-ph]]; M. C. Kumar, P. Mathews,

V. Ravindran and A. Tripathi, Phys. Lett. B **672** (2009) 45 [arXiv:0811.1670 [hep-ph]].

[13] P. Mathews, V. Ravindran, K. Sridhar and W. L. van Neerven, Nucl. Phys. B **713**, 333 (2005) [arXiv:hep-ph/0411018]. P. Mathews, V. Ravindran and K. Sridhar, JHEP **0510**, 031 (2005) [arXiv:hep-ph/0506158]. P. Mathews and V. Ravindran, Nucl. Phys. B **753**, 1 (2006) [arXiv:hep-ph/0507250]. M. C. Kumar, P. Mathews and V. Ravindran, Eur. Phys. J. C **49**, 599 (2007) [arXiv:hep-ph/0604135].

[14] A. Abulencia *et al.* [CDF Collaboration], Phys. Rev. Lett. **97** (2006) 171802 [arXiv:hep-ex/0605101].

[15] V. M. Abazov *et al.* [D0 Collaboration], Phys. Rev. Lett. **100** (2008) 091802 [arXiv:0710.3338 [hep-ex]].

[16] M. C. Kumar, P. Mathews, V. Ravindran and A. Tripathi, Phys. Rev. D **77** (2008) 055013 [arXiv:0709.2478 [hep-ph]]; M. C. Kumar, P. Mathews, V. Ravindran and A. Tripathi, arXiv:0804.4054 [hep-ph];

[17] M. C. Kumar, P. Mathews, V. Ravindran and A. Tripathi, Phys. Lett. B **672** (2009) 45 [arXiv:0811.1670 [hep-ph]].

[18] FORM by J.A.M. Vermaseren, version 3.0 available from http://www.nikhef.nl/form.

[19] L.J. Bergmann, Next-to-leading-log QCD calculation of symmetric dihadron production, Ph.D. thesis, Florida State University, 1989; L. Bergmann and J.F. Owens, Report No. FSU-HEP-890601 (unpublished).

[20] B. Bailey, J. F. Owens and J. Ohnemus, Phys. Rev. D **46** (1992) 2018.

[21] B. W. Harris and J. F. Owens, Phys. Rev. D **65** (2002) 094032 [arXiv:hep-ph/0102128].

[22] R. K. Ellis, I. Hinchliffe, M. Soldate and J. J. van der Bij, Nucl. Phys. B **297** (1988) 221; L. Ametller, E. Gava, N. Paver and D. Treleani, Phys. Rev. D **32**, 1699 (1985); D.A. Dicus and S.S.D. Willenbrock, Phys. Rev. D **37**, 1801 (1988).

[23] S. Frixione, Phys. Lett. B **429** (1998) 369.

[24] ATLAS Collaboration, ATLAS detector and physics performance. Technical design report. Vol. 2 (1999), CERN-LHCC-99-15.

[25] CMS Collaboration, "CMS: The electromagnetic calorimeter, technical design report," report CERN/LHCC 97-33, CMS-TDR-4.

[26] J. Pumplin *et al.*, JHEP **0207** (2002) 012.

Figure 1: Born contributions

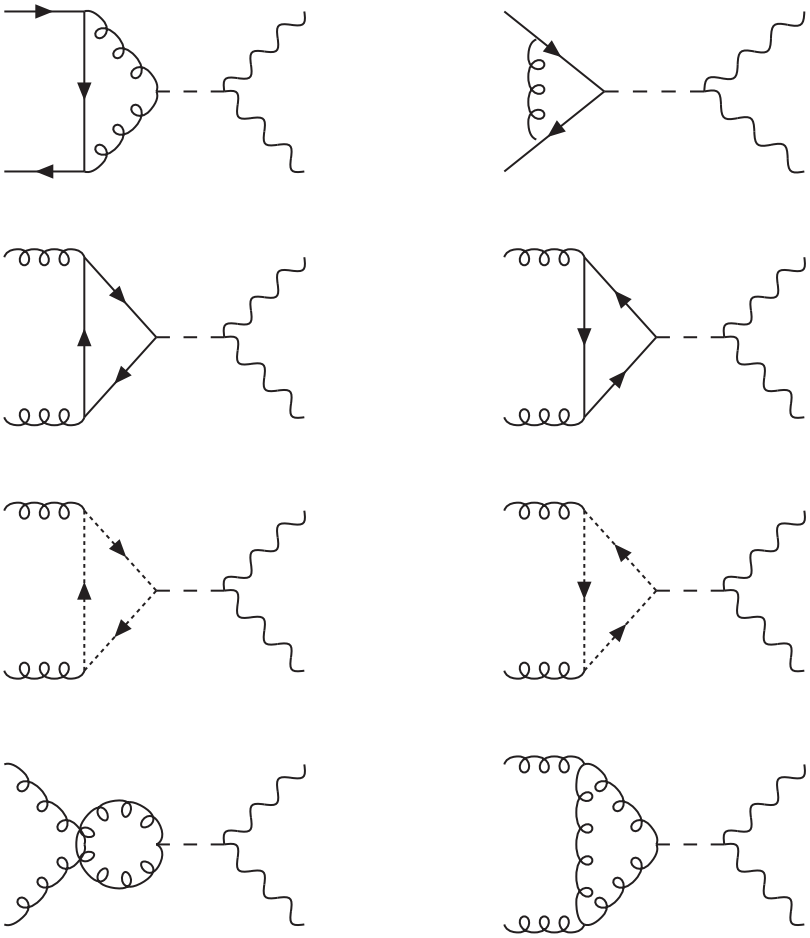

Figure 2: Virtual contributions

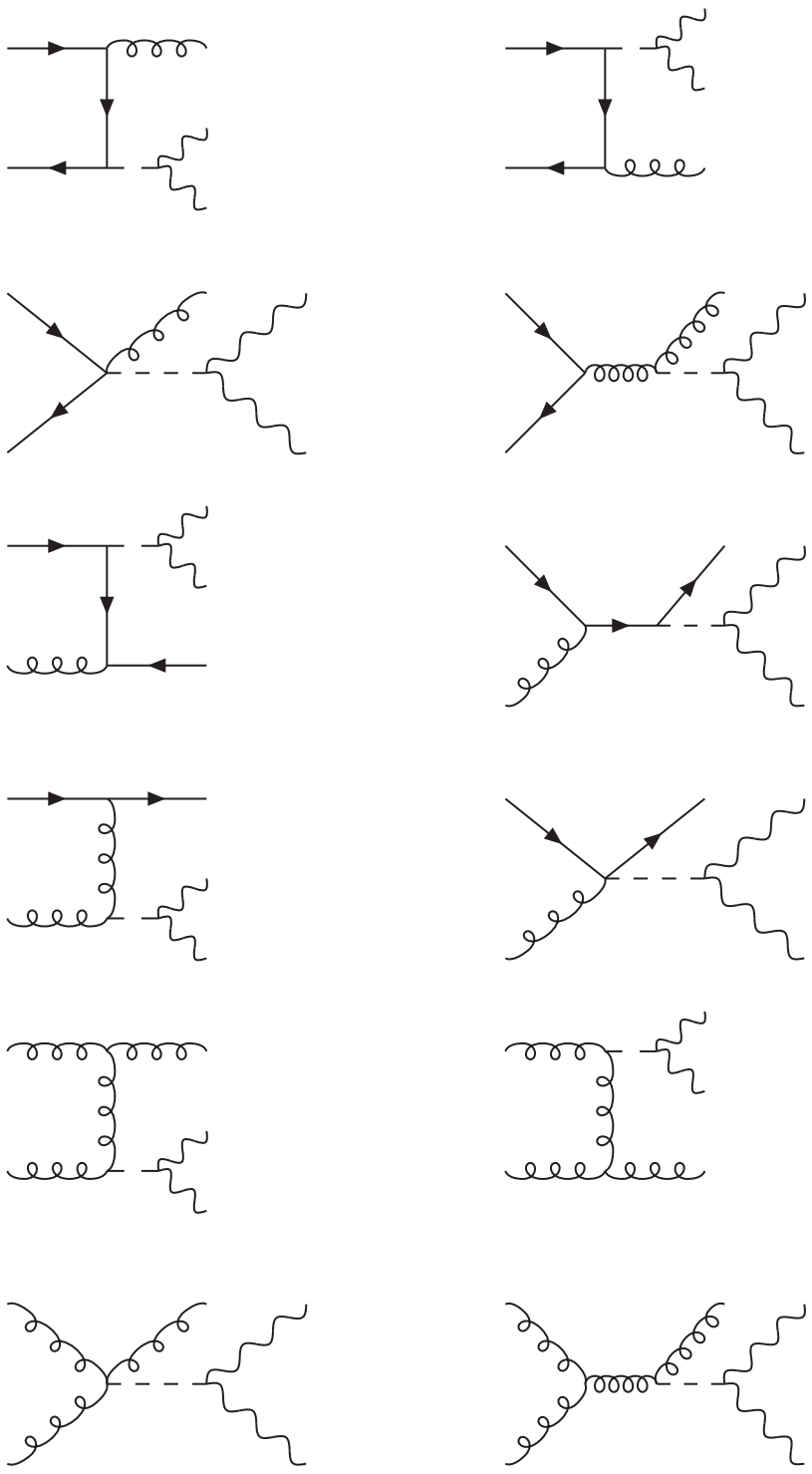

Figure 3: Real emission contributions

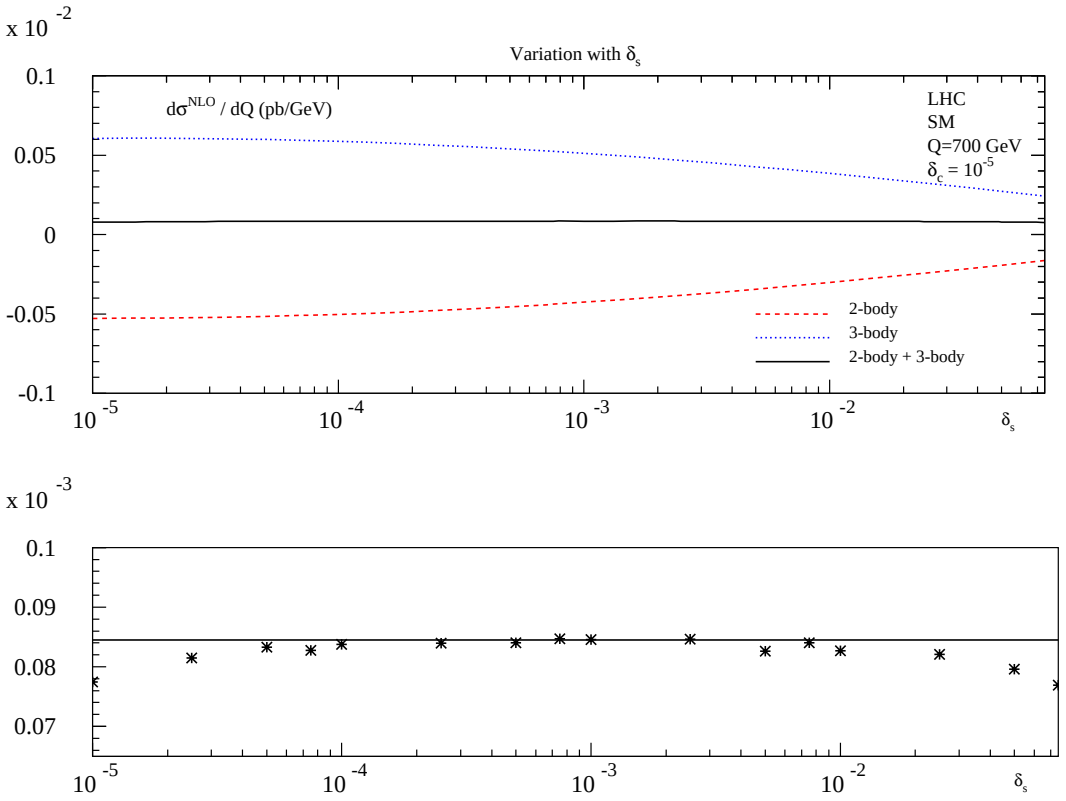

Figure 4: Stability of the order α_s contribution to the SM cross section against the variation of the slicing parameter δ_s (top), with $\delta_c = 10^{-5}$ fixed, in the invariant mass distribution of the di-photon. Below is shown the variation of the sum of 2-body and 3-body contributions over the range of δ_s considered and contrasted against the one at $\delta_s = 10^{-3}$.

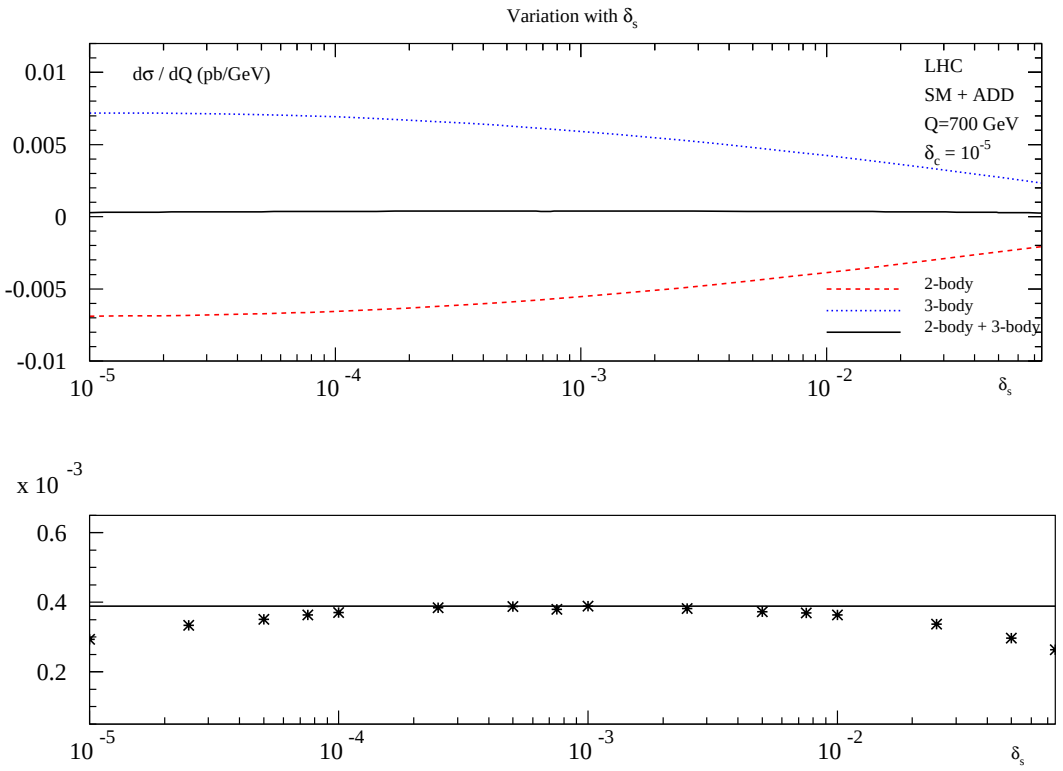

Figure 5: Stability of the order α_s contribution to the SM+ADD cross section against the variation of the slicing parameter δ_s (top), with $\delta_c = 10^{-5}$ fixed, in the invariant mass distribution of the di-photon with $M_S = 2$ TeV and $d = 3$. Below is shown the variation of the sum of 2-body and 3-body contributions over the range of δ_s considered and contrasted against the one at $\delta_s = 10^{-3}$.

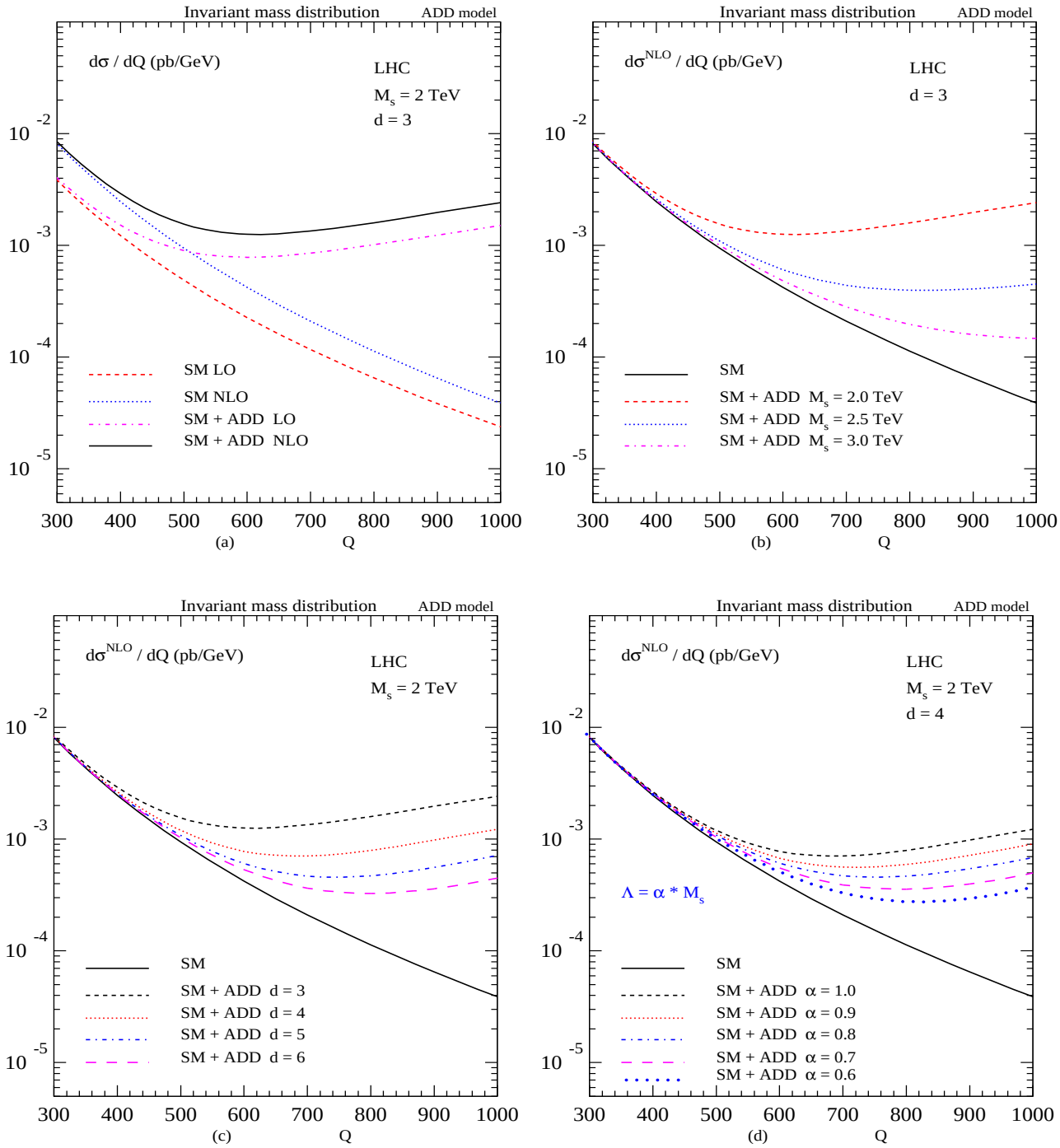

Figure 6: Invariant mass distribution of the di-photon production in the ADD model at the LHC. In (a) both SM and the signal (SM+ADD) are presented at LO and NLO for $M_S = 2$ TeV and $d = 3$. Further the dependency of the cross sections on the scale M_S in (b), on the number d of extra dimensions in (c) and on the cut-off scale Λ for the summation over virtual KK modes in (d), has been shown to NLO in QCD.

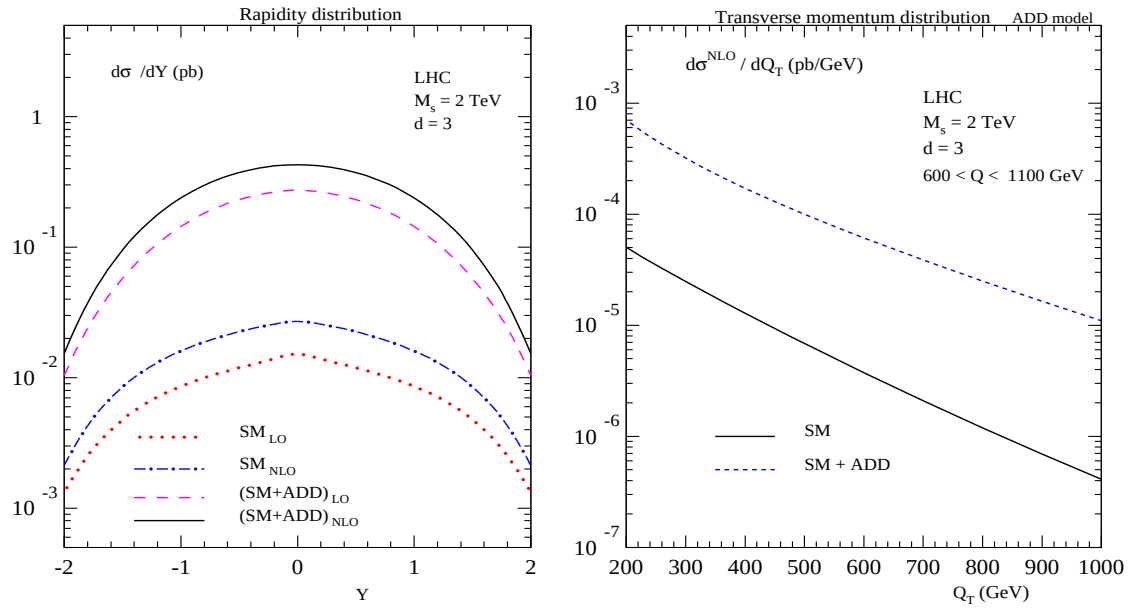

Figure 7: Transverse momentum rapidity $d\sigma/dY$ (left) and $d\sigma/dQ_T$ (right) distributions of the di-photon production are presented in the ADD model with $M_S = 2$ TeV, $d = 3$ and by integrating over Q in the range $600 < Q < 1100$ GeV.

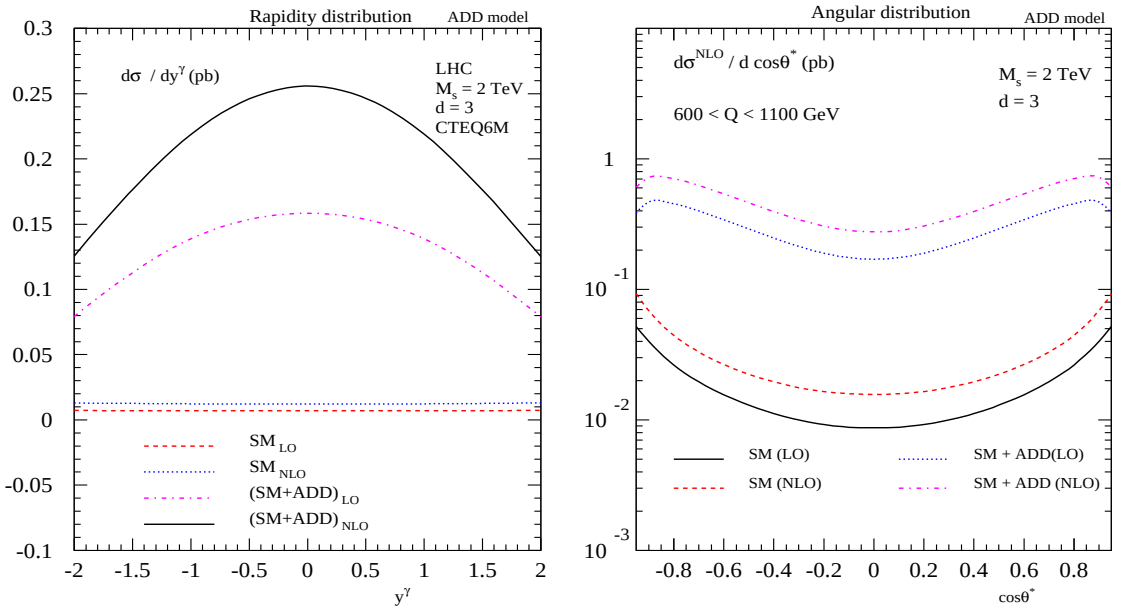

Figure 8: Rapidity $d\sigma/dy^\gamma$ (left) and angular distributions $d\sigma/d\ \cos\theta^*$ (right) of the photons are presented in the ADD model with $M_S = 2$ and $d = 3$. Both of these distributions are obtained by integrating over the invariant mass of the di-photon in the range $600 < Q < 1100$ GeV.

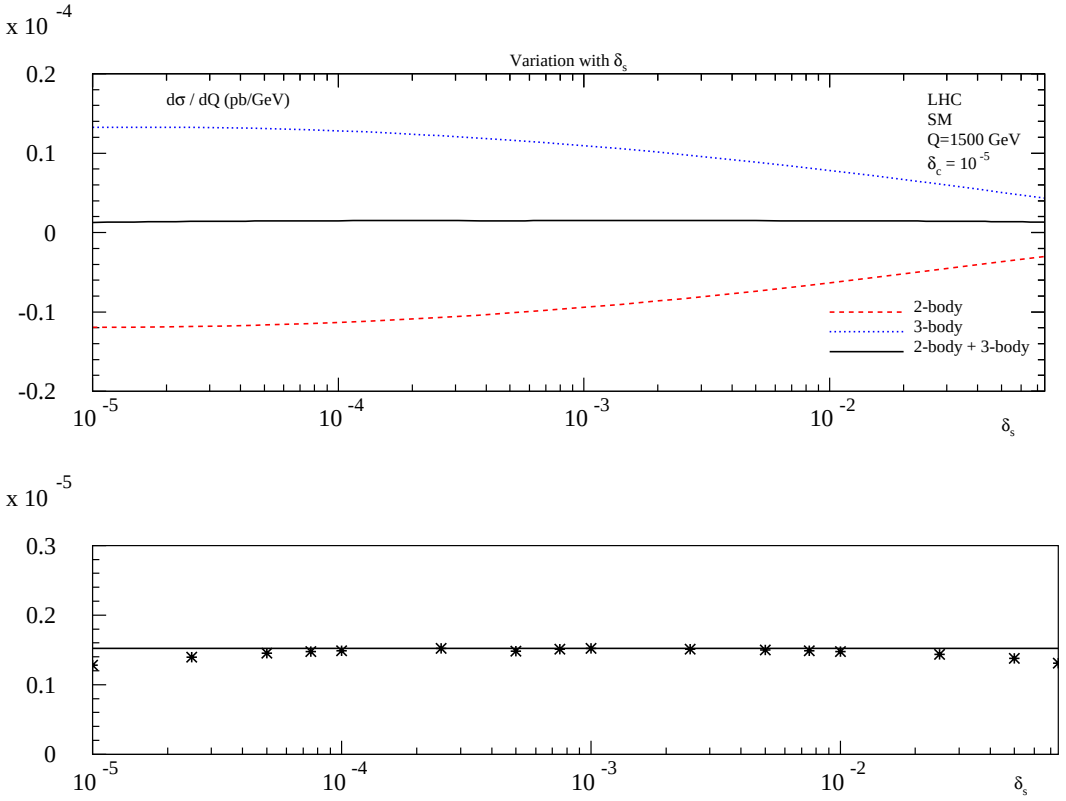

Figure 9: Stability of the order α_s contribution to the SM cross section against the variation of the slicing parameter δ_s (top), with $\delta_c = 10^{-5}$ fixed, in the invariant mass distribution of the di-photon. Below is shown the variation of the sum of 2-body and 3-body contributions over the range of δ_s considered and contrasted against the one at $\delta_s = 10^{-3}$.

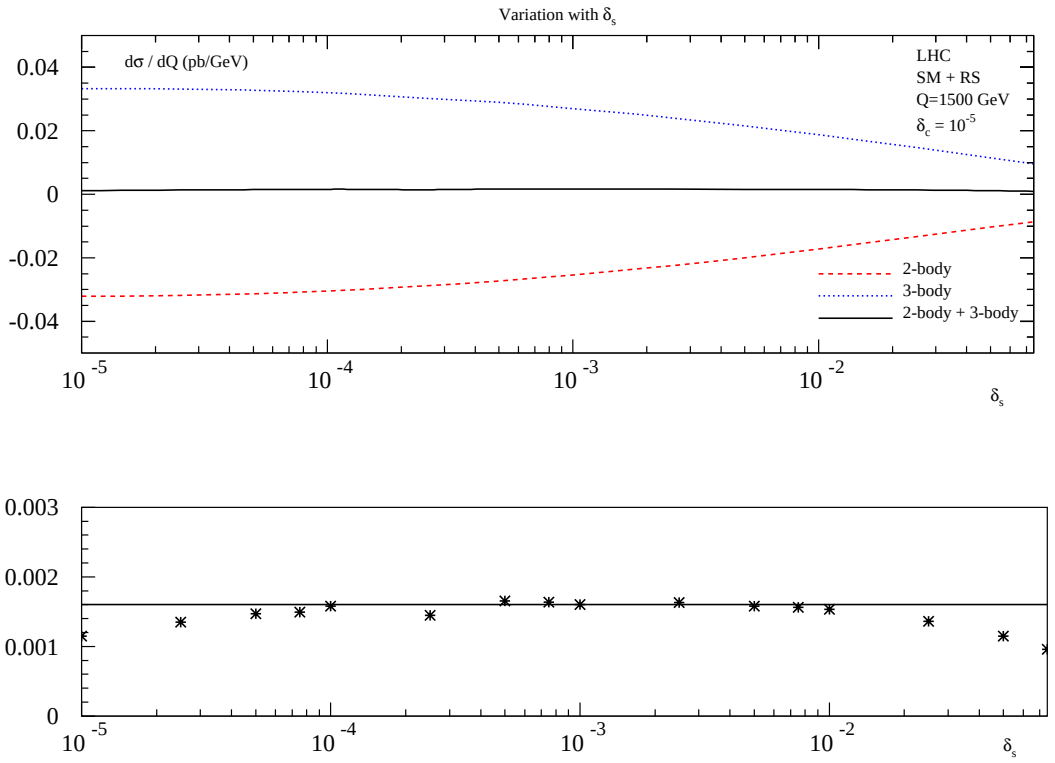

Figure 10: Stability of the order α_s contribution to the SM+RS cross section against the variation of the slicing parameter δ_s (top), with $\delta_c = 10^{-5}$ fixed, in the invariant mass distribution of the di-photon with $M_1 = 1.5$ TeV and $c_0 = 0.01$. Below is shown the variation of the sum of 2-body and 3-body contributions over the range of δ_s considered and contrasted against the one at $\delta_s = 10^{-3}$.

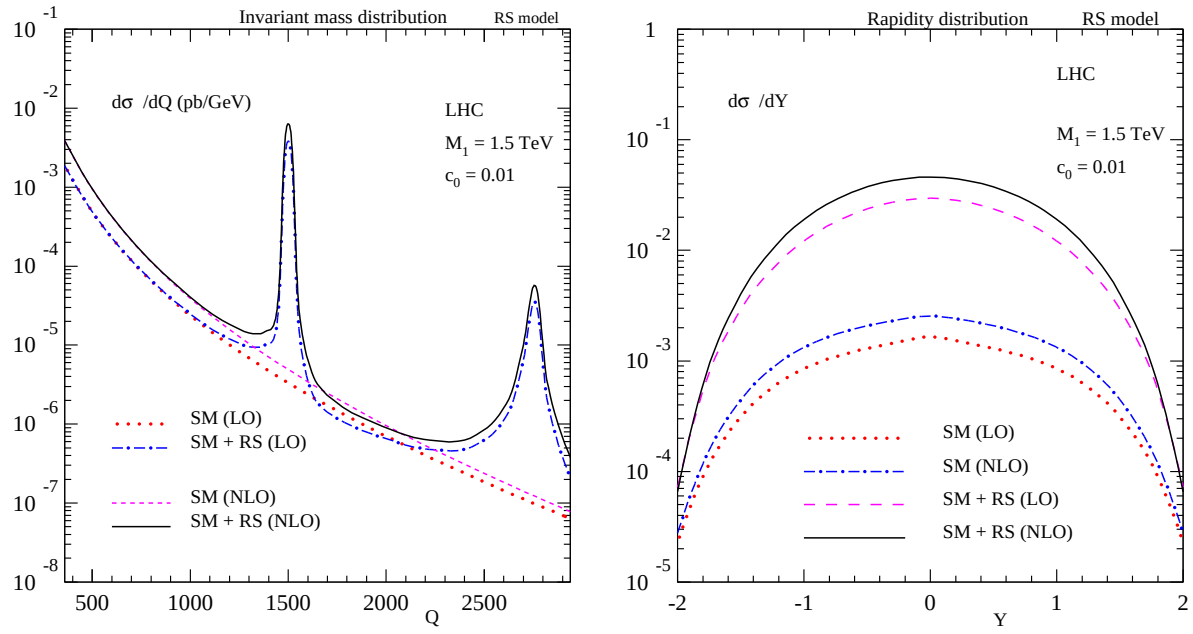

Figure 11: Invariant mass $d\sigma/dQ$ (left) and rapidity $d\sigma/dY$ (right) distributions of the di-photon production in the RS model with $M_1 = 1.5$ TeV and $c_0 = 0.01$ at the LHC.

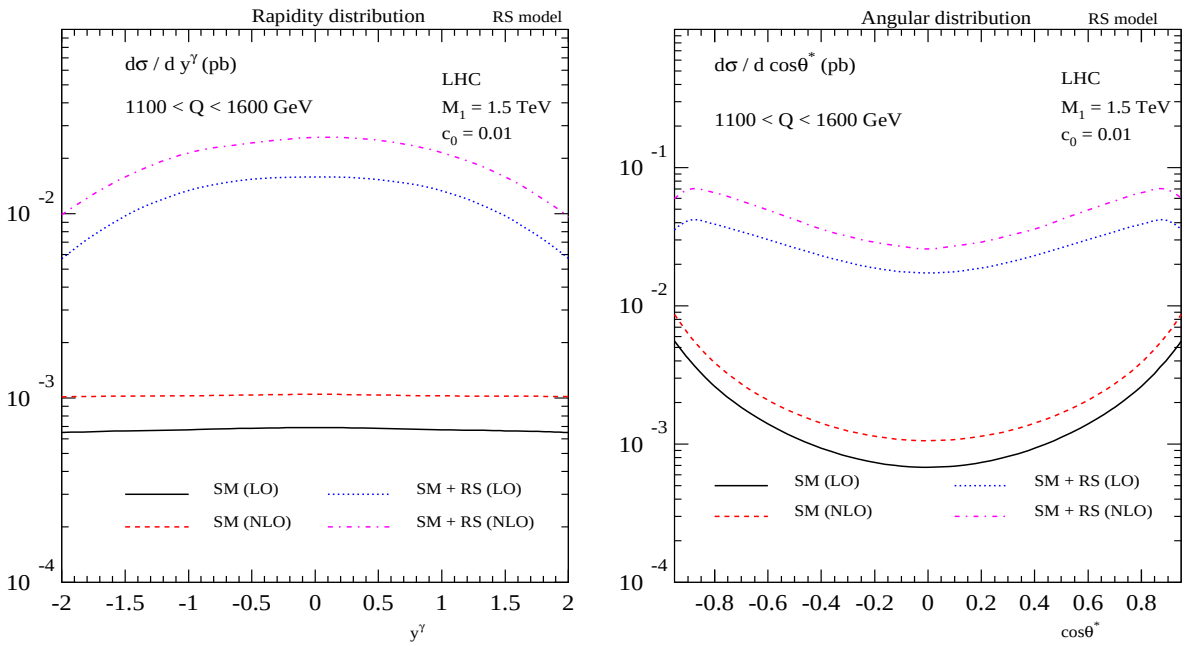

Figure 12: Rapidity $d\sigma/dy^\gamma$ (left) and angular $d\sigma/d\ \cos\theta^*$ (right) distributions of the photons in the RS model with $M_1 = 1.5$ TeV and $c_0 = 0.01$ at the LHC.

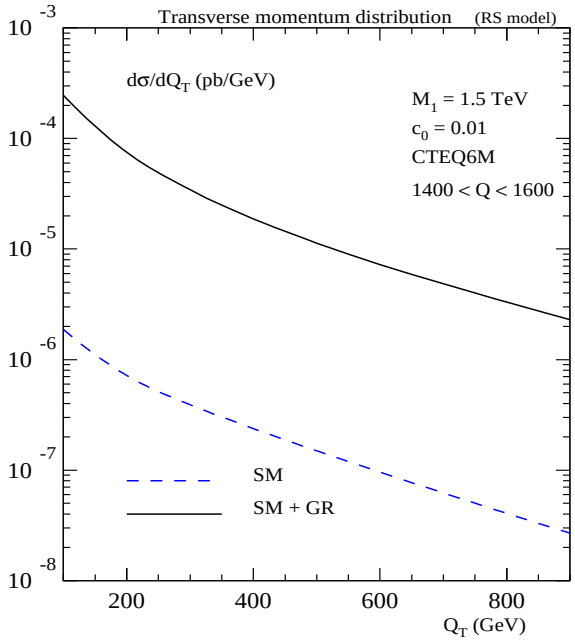

Figure 13: Transverse momentum distribution of the di-photon production in the RS model with $M_1 = 1.5$ TeV and $c_0 = 0.01$. Here we have integrated over Q around the first resonance region $1100 \leq Q \leq 1600$ GeV.

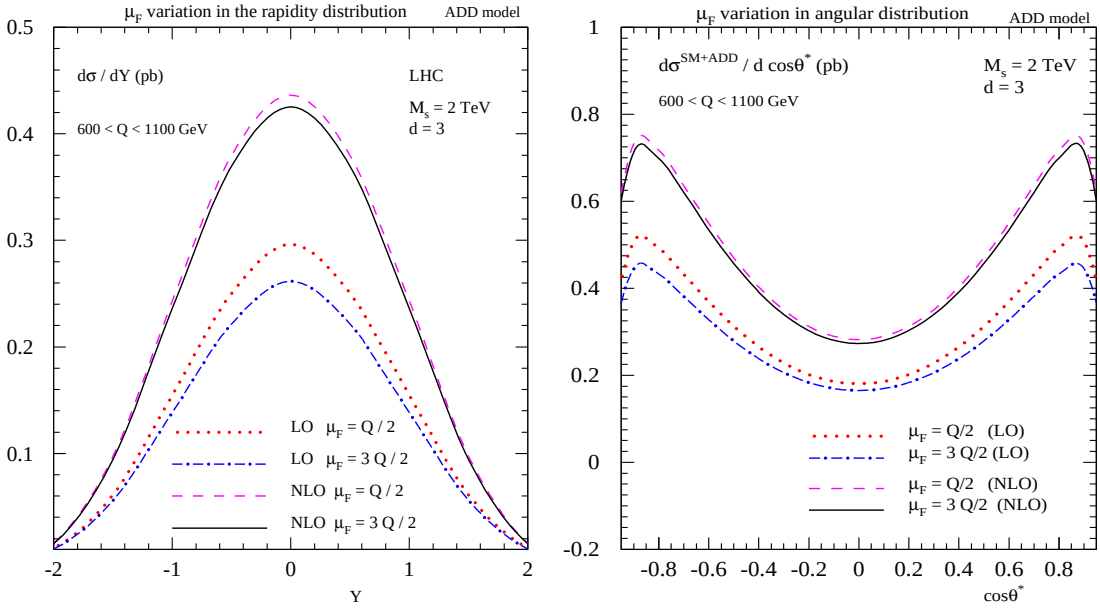

Figure 14: Factorization scale dependency of the LO and NLO cross sections in the ADD model with $M_S = 2$ TeV and $d = 3$ for a scale variation of $Q/2 < \mu_F < 3Q/2$. For both the rapidity (left) and angular (right) distributions of the di-photon production, we have integrated over the invariant mass in the range $600 < Q < 1100$ GeV.

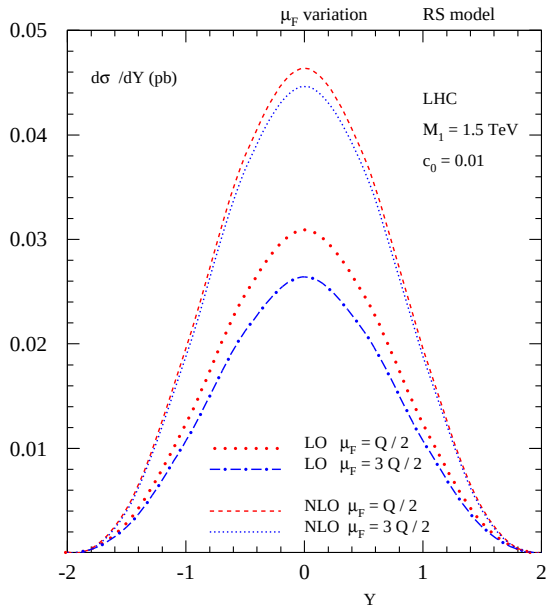

Figure 15: The factorization scale dependency is shown in the rapidity distribution $d\sigma/dY$ of the di-photon for a scale variation of $Q/2 \leq \mu_F \leq 3Q/2$. For this distribution we have integrated over the invariant mass of the di-photon in the range $1100 \leq Q \leq 1600$ GeV.